High-harmonic generation in gases and solids

A. Thorpe,[1,*] N. Boroumand,[1] G. Bart,[1] L. Wang,[1] G. Vampa,[1,2] and T. Brabec[1]
[1]*Department of Physics, University of Ottawa, Ontario K1N 6N5, Canada*
[2]*National Research Council of Canada, Ottawa, Ontario K1A 0R6, Canada*

(Received 19 August 2025; accepted 13 November 2025; published 10 December 2025)

We present a quantum optical generalization of the quantum-matter Lewenstein model of high-harmonic generation (HHG) in gases that contains two channels corresponding to the inter and intraband HHG in solids. Both channels can be presented as a semiclassical current multiplied by the vacuum field strength, resulting in a quantitative correction and a faster roll-off of the harmonic power with order than in previous theories. In gases, like in solids, intraband HHG dominates at low orders; the switchover harmonic corresponds to a specific photon energy, independent of pump wavelength.

DOI: 10.1103/8lhh-gq58

I. INTRODUCTION

Theories of the interaction of intense electromagnetic radiation with matter predate the widespread use of intense laser sources [1–3]. One strong-field laser phenomenon, high-harmonic generation (HHG), was initially observed in gases during the late 1980s and early 1990s [4–6] and has since been extensively investigated for its applications, such as providing a source of ultrafast coherent light and applications in attosecond spectroscopy [7–10].

The exploration of HHG has expanded to solids [11], offering an extension of attosecond science to convenient tabletop media [10,12–16]. HHG in solids had allowed for applications like probing various aspects of electronic band structure [17–20], imaging transition dipole moments [21] and Berry curvatures [22–24], as well as topological states of matter [25,26] and phase transitions [27].

Recently, there has been growing interest in the quantum optical aspects of HHG. This has opened a number of applications, such as generation of Schrödinger cat states [28–30], photon bunching and antibunching [31–37], and generation of squeezed light [35–37] from HHG with classical and nonclassical light sources, such as bright squeezed vacuum [38–43]. It has also been shown that bound states may influence the quantum nature of the emitted high-harmonic (HH) radiation [44,45].

HHG is typically elucidated in atomic gases according to Lewenstein's seminal work [46]. This semiclassical approach—treating light classically and matter quantum mechanically—considers oscillations of a field-induced bound-continuum state dipole. It has an intuitive three-step explanation: An electron is ionized by a strong laser field, then propagates within the field-dressed continuum, and finally recombines with an ionic core, converting its excess energy into ultrafast pulses of light with odd frequency multiples of the driving laser's frequency [9,46–48]. A similar mechanism has been studied in solids, known as the interband mechanism, where an electron is excited to a conduction band and a hole is promoted to a valence band, and they propagate before recombining to emit HH light [12,49,50,51].

In addition to the interband mechanism, there also exists an intraband mechanism in solids [12,49]. This mechanism describes the generation of harmonics as a response to charge motion within individual electronic bands. The relation between the two mechanisms in atoms, analogous to interband and intraband HHG in solids, has not been explored yet.

Finally, while semiclassical models reproduce HHG spectra qualitatively very well, they are not quantitatively accurate. This limitation arises from their neglect of vacuum electric field fluctuations, which are essential for a full quantum description.

Here, we develop a quantum optical generalization of the quantum-matter Lewenstein model, which yields the following insights.

First, the quantum optical strong-field model inherently contains interband and intraband currents for both gases and solids. As such, it allows for a one-to-one connection between HHG in gases and solids. In atoms, the intraband mechanism is related to Brunel HHG [52].

Second, the quantum optical Lewenstein model yields semiclassical currents multiplied by the vacuum electric field. This is lost in semiclassical approaches, and allows for a close to quantitative description of HHG, as long as a Coulomb correction factor to ionization is included, and bound states can be neglected.

Third, due to the frequency dependence of the vacuum electric field, the frequency scaling of HHG is also different from semiclassical theories. This results in a faster decrease of the harmonic power with order than in previous theories.

*Contact author: athor087@uottawa.ca

Fourth, our analysis shows that, like in solids, the intraband current in atomic gases is important. It is the dominant source for low-order HHG in atomic and molecular gases. Provided ionization is well into the tunneling regime, the crossover harmonic between interband and intraband HHG relates to a specific photon energy independent of the pump laser wavelength.

Finally, the computational efficiency of the quantum optical Lewenstein model, in particular after using saddle point integration [53], allows for efficient integration into macroscopic phase matching models and thus, a scalable, close to quantitative description of HHG experiments in atomic and molecular gases. This makes it a valuable tool for the design and interpretation of experiments.

II. DERIVATION OF THE PHOTON WAVEFUNCTION

To model the problem, we introduce the Hamiltonian $\hat{H} = \hat{H}_m + \hat{H}_f + \hat{H}_i$, where

$$\hat{H}_m = \frac{\hat{\mathbf{p}}^2}{2m} + V(\mathbf{r}), \tag{1}$$

$$\hat{H}_f = \sum_\kappa \hbar\omega_k \hat{a}_\kappa^\dagger \hat{a}_\kappa, \tag{2}$$

$$\hat{H}_i = \mathbf{r}|e|\hat{\mathbf{F}}(\mathbf{x}) \tag{3}$$

are the matter, field, and interaction Hamiltonians, respectively. Here, $\hat{\mathbf{p}}$ represents the momentum operator, $\mathbf{r}$ defines the relative coordinates, and $\mathbf{x}$ defines the center of mass coordinates. Further, m and $|e|$ define the electronic mass and charge, respectively. The creation and annihilation operators $\hat{a}_\kappa^\dagger$ and $\hat{a}_\kappa$ correspond to the electromagnetic field mode $\kappa \equiv (\mathbf{k}, s)$, with wavevector $\mathbf{k}$ and $s = 1$ or 2 labeling two orthogonal unit vectors that define the polarization basis of the light field. The quantized electric field and vector potential are given by

$$\hat{\mathbf{F}}(\mathbf{x}) = i\sum_\kappa \eta_\kappa\omega_\kappa \mathbf{e}_\kappa(\hat{a}_\kappa e^{i\mathbf{kx}} - \hat{a}_\kappa^\dagger e^{-i\mathbf{kx}}), \tag{4a}$$

$$\hat{\mathbf{A}}(\mathbf{x}) = \sum_\kappa \eta_\kappa \mathbf{e}_\kappa(\hat{a}_\kappa e^{i\mathbf{kx}} + \hat{a}_\kappa^\dagger e^{-i\mathbf{kx}}), \tag{4b}$$

respectively, where $\mathbf{e}_\kappa$ is the unit vector along the polarization direction, $\eta_\kappa = \sqrt{\hbar/(2\omega_k\varepsilon_0 V)}$ is the vacuum vector field amplitude, ω_k is the mode frequency, ε_0 is the vacuum permittivity, and V is the quantization volume.

We use the strong field and dipole approximations, considering a hydrogen-like atom with a ground state $|0\rangle$ and continuum states $|\mathbf{p}\rangle = 1/(2\pi\hbar)^{3/2}\exp((i/\hbar)\mathbf{pr})$ [1,10,54]. Doing so, we utilize the Ansatz

$$|\Psi(t)\rangle = |0\rangle \otimes |\phi_0(t)\rangle + \int d^3p|\mathbf{p}\rangle \otimes |\phi_\mathbf{p}(t)\rangle, \tag{5}$$

where photon quantum states $|\phi_0(t)\rangle$ and $|\phi_\mathbf{p}(t)\rangle$ are associated with the ground and continuum states, respectively. By determining the evolution of $|\phi_0(t)\rangle$ with the Schrödinger equation,

$$i\hbar\partial_t|\Psi(t)\rangle = \hat{H}|\Psi(t)\rangle = (\hat{H}_m + \hat{H}_f + \hat{H}_i)|\Psi(t)\rangle, \tag{6}$$

we can measure HHG using the photon number expectation value $\langle\hat{n}\rangle(t) \approx \langle\phi_0(t)|\hat{n}|\phi_0(t)\rangle$. To measure HHG, Eq. (5) can be generalized to many atoms [43], but for clarity, we highlight the single-atom case here.

We simplify solving the Schrödinger equation by using the transformation $|\varphi_l(t)\rangle = \hat{D}_\alpha^\dagger\hat{U}_v^\dagger\hat{U}_i^\dagger|\phi_l(t)\rangle$ ($l = 0, \mathbf{p}$), where

$$\hat{U}_i = \exp(-i\hat{H}_f t/\hbar), \tag{7}$$

$$\hat{U}_v = \exp(i|e|\mathbf{r}\hat{\mathbf{A}}/\hbar), \tag{8}$$

$$\hat{D}_\alpha = \exp\left(\sum_\kappa \alpha_\kappa\hat{a}_\kappa^\dagger - \alpha_\kappa^*\hat{a}_\kappa\right) \tag{9}$$

consist of the interaction picture operator, the velocity gauge operator, and the displacement operator over modes of the driving laser field, respectively. Here, α_κ corresponds to the single-mode complex coherent state amplitudes. This separates the strong driving laser field and quantum optical fields, excluding the fundamental harmonic in HHG analysis. The electric field splits into $\tilde{\mathbf{F}}(t) = \boldsymbol{\mathcal{F}}(t) + \hat{\mathbf{F}}(t)$, with $\boldsymbol{\mathcal{F}}(t)$ treated classically and $\hat{\mathbf{F}}(t)$ quantum optically. Similarly, $\tilde{\mathbf{A}}(t) = \boldsymbol{\mathcal{A}}(t) + \hat{\mathbf{A}}(t)$ and Rabi frequency $\tilde{\Omega}(t) = |e|\mathbf{d}(\mathbf{p}_t)\tilde{\mathbf{F}}(t)/\hbar = \Omega(t) + \hat{\Omega}(t)$ with $\mathbf{p}_t = \mathbf{p} + |e|\boldsymbol{\mathcal{A}}(t)$ and transition dipole moment $\mathbf{d}(\mathbf{p}) = \langle\mathbf{p}|\mathbf{r}|0\rangle$ [54,55]. Evaluating the Schrödinger equation leads to the coupled differential equations,

$$i\hbar\partial_t|\varphi_0(t)\rangle = E_0|\varphi_0(t)\rangle + \hbar\int d^3p\,\tilde{\Omega}^\dagger(t)\,|\varphi_\mathbf{p}(t)\rangle, \tag{10a}$$

$$\begin{aligned} i\hbar\partial_t|\varphi_\mathbf{p}(t)\rangle = {} & \left(\frac{1}{2m}\mathbf{p}_t^2 + \frac{|e|}{m}\mathbf{p}_t\hat{\mathbf{A}}(t)\right)|\varphi_\mathbf{p}(t)\rangle \\ & + \hbar\tilde{\Omega}(t)\,|\varphi_0(t)\rangle. \end{aligned} \tag{10b}$$

In the process of obtaining of Eq. (10), we noted that the quantum fields clearly present a perturbation to the intense pump field. As a result, we introduced the following approximations: (1) We expanded the dipole moments with regard to the operator arguments to first order, $\mathbf{d}(\mathbf{p}_t + |e|\hat{\mathbf{A}}(t)) \approx \mathbf{d}(\mathbf{p}_t) + |e|[(\hat{\mathbf{A}}(t)\nabla_\mathbf{p})\mathbf{d}(\mathbf{p})]_{\mathbf{p}_t}$, where $\mathbf{p}_t = \mathbf{p} + |e|\boldsymbol{\mathcal{A}}(t)$. While we do not carry along the first-order contribution in this work, we keep in mind that it is there. (2) We approximated $(\mathbf{p} + |e|\tilde{\mathbf{A}}(t))^2 \approx \mathbf{p}_t^2 + 2\mathbf{p}_t|e|\hat{\mathbf{A}}(t)$.

Equation (10b) is integrated by using the Ansatz

$$|\varphi_\mathbf{p}(t)\rangle = \hat{D}_\sigma(t)\,\exp\left(i\int_{t_0}^t g' dt'\right)|\tilde{\varphi}_\mathbf{p}(t)\rangle, \tag{11}$$

where the displacement operator

$$\hat{D}_\sigma^\dagger(t) = \exp\left(-\sum_\kappa \sigma_\kappa\hat{a}_\kappa^\dagger - \sigma_\kappa^*\hat{a}_\kappa\right) \tag{12}$$

consists of

$$\sigma_\kappa(t) = \frac{|e|E_v}{\hbar}\overline{\sigma}_\kappa(t)e^{-i(\mathbf{kx}-\omega_k t)}, \tag{13}$$

$$\overline{\sigma}_\kappa(t) = \frac{-i}{m\omega_k}\int_{t_0}^t \mathbf{e}_\kappa\mathbf{p}_{t'}e^{-i\omega_k(t-t')}dt', \tag{14}$$

with $E_v = \omega_k\eta_\kappa$ as the vacuum electric field amplitude, $\sigma_\kappa(t)$ defines the dressing of continuum electrons with coherent state radiation modes. Finally, the phase contribution is determined by

$$ig'(t) = \frac{1}{2}\left[-i\frac{|e|}{\hbar m}\int_{t_0}^{t} dt' \mathbf{p}_{t'}\hat{\mathbf{A}}(t'), -i\frac{|e|}{\hbar m}\mathbf{p}_t\hat{\mathbf{A}}(t)\right] = i\sum_{\kappa}\mathrm{Im}[\dot{\sigma}_\kappa^*(t)\sigma_\kappa(t)]. \quad (15)$$

As a result of Ansatz Eq. (11) with Eq. (10b), after transforming back we find,

$$|\varphi_{\mathbf{p}}(t)\rangle = -i\int_{t_0}^{t} dt' \exp\left(-\frac{i}{2m\hbar}\int_{t'}^{t}\mathbf{p}_\tau^2 d\tau + ig(t',t)\right) \times \tilde{\Omega}(t')\hat{D}_\sigma(t',t)|\varphi_0(t')\rangle, \quad (16)$$

where

$$g(t',t) = \int_{t'}^{t} g'(\tau)d\tau + g''(t',t) \quad (17)$$

with,

$$g''(t',t) = \frac{i}{2}\left(\frac{|e|}{\hbar m}\right)^2\left[\int_{t_0}^{t} d\tau \mathbf{p}_\tau\hat{\mathbf{A}}(\tau), \int_{t_0}^{t'} d\tau \mathbf{p}_\tau\hat{\mathbf{A}}(\tau)\right] = \sum_{\kappa}\mathrm{Im}[\sigma_\kappa(t')\sigma_\kappa^*(t)] \quad (18)$$

is a quantum vacuum phase term that can be neglected (see Appendix B of the Supplemental Material [55]).

Using Eqs. (10a) and (16), we arrive at the Volterra integro-differential equation

$$\partial_t|\varphi_0(t)\rangle = -\int d^3p\,\hat{c}_{\mathbf{p}}^\dagger(t)\int_{t_0}^{t} dt'\hat{c}_{\mathbf{p}}(t')|\varphi_0(t')\rangle, \quad (19)$$

where

$$\hat{c}_{\mathbf{p}}(t) = \tilde{\Omega}(t)\hat{D}_\sigma^\dagger(t)\exp(iS(t)) \quad (20)$$

with

$$S(t) = \frac{1}{\hbar}\int_{t_0}^{t}\left(\frac{\mathbf{p}_\tau^2}{2m} + E_0\right)d\tau \quad (21)$$

the classical action.

III. ONE-PHOTON OPERATOR CONTRIBUTION

While numerical methods [37] like the variational iteration method (see Ref. [56]) can solve equations like Eq. (19), we use a simpler approximation for clarity. Following the Lewenstein approach for ground state depletion, we assume the photon wavefunction varies slowly and can be extracted from the integral [46]. The resulting differential equation of motion is

$$\partial_t|\varphi_0(t)\rangle \approx (\partial_t\hat{\mathfrak{h}}(t))|\varphi_0(t)\rangle. \quad (22)$$

Integration of Eq. (22) by the method of Magnus and Fer [57] results in

$$|\varphi_0(t)\rangle \approx \exp(\hat{\mathfrak{h}}(t))|\varphi_0(t_0)\rangle, \quad (23)$$

$$\hat{\mathfrak{h}} = -\int d^3p\int_{t_0}^{t} dt'\,\hat{c}_{\mathbf{p}}^\dagger(t')\int_{t_0}^{t'} dt''\,\hat{c}_{\mathbf{p}}(t''), \quad (24)$$

with higher-order Magnus and Fer expansion contributions neglected.

Additionally, assuming first-order expansion of the operator expressions in Eq. (24), we find, after integration by parts,

$$\hat{\mathfrak{h}}^{(1)} \approx \int d^3p\int_{t_0}^{\infty} dt'\left(\hat{c}_{\mathbf{p}}^{(1)}\hat{C}_{\mathbf{p}}^{(0)*} - \hat{c}_{\mathbf{p}}^{(1)\dagger}\hat{C}_{\mathbf{p}}^{(0)}\right)(t'), \quad (25)$$

where we also have let $t \to \infty$. Further,

$$\hat{c}_{\mathbf{p}}^{(0)}(t) = \Omega(t)e^{iS(t)}, \quad (26)$$

$$\hat{c}_{\mathbf{p}}^{(1)}(t) = \sum_{\kappa}(\hat{\Omega}_\kappa(t) - \Omega(t)\hat{\sigma}_\kappa(t))e^{iS(t)} \quad (27)$$

represent zero- and first-order expansion components of $\hat{c}_{\mathbf{p}}$ in terms of creation and annihilation operators, and we have introduced $\hat{C}_{\mathbf{p}}^{(j)}(t) = \int_{-\infty}^{t} dt'\hat{c}_{\mathbf{p}}^{(j)}(t')$ $(j = 0, 1)$. In Eq. (27), $\hat{\sigma}_\kappa(t) = \sigma_\kappa(t)\hat{a}_\kappa^\dagger - \sigma_\kappa^*(t)\hat{a}_\kappa$, and $\hat{\Omega}_\kappa(t)$ is the κ mode component of $\hat{\Omega}(t)$.

Finally, using Eqs. (25) and (23), we find that the ground-state photon wavefunction can be worked out to be,

$$|\varphi_0(t)\rangle \approx \exp\left(\sum_{\kappa} h_\kappa\hat{a}_\kappa^\dagger - h_\kappa^*\hat{a}_\kappa\right)|\varphi_0(t_0)\rangle, \quad (28)$$

where h_κ is the coherent state parameter that we will define in Eqs. (29) and (30) below. Assuming the initial state of the system is vacuum $|\varphi_0(t_0)\rangle = |v\rangle$, Eq. (28) represents a coherent state.

IV. CONNECTION TO SEMICLASSICAL ANALYSIS OF HHG

A. Connection to Lewenstein's model

To connect with semiclassical analysis of HHG, the coherent state parameter $h_\kappa = h'_\kappa + h''_\kappa$ involves two channels

$$h'_\kappa = \frac{|e|E_v}{\hbar}\mathbf{e}_\kappa\int_{-\infty}^{\infty} dt\,e^{i(\omega_k t - \mathbf{kx})}\mathbf{x}(t), \quad (29)$$

$$h''_\kappa = -\frac{|e|E_v}{\hbar}\int_{-\infty}^{\infty} dt\,e^{i(\omega_k t - \mathbf{kx})}\int d^3p\,\bar{\sigma}_\kappa(t)[\Gamma_{\mathbf{p}}(t) + \mathrm{c.c.}], \quad (30)$$

with

$$\mathbf{x}(t) = 2\mathrm{Re}\left[i\int d^3p\,\mathbf{d}^*(\mathbf{p}_t)e^{-iS(t)}\int_{-\infty}^{t} dt'\Omega(t')e^{iS(t')}\right], \quad (31)$$

$$\Gamma_{\mathbf{p}}(t) = \Omega^*(t)e^{-iS(t)}\int_{-\infty}^{t} dt'\Omega(t')e^{iS(t')}. \quad (32)$$

Here, $\mathbf{x}(t)$ in Eq. (31) is Lewenstein's time-dependent dipole, which describes charge oscillations due to polarization buildup between the atomic ground state and electronic continuum states [46]. Equation (32) is the momentum-dependent complex ionization rate, related to the full complex ionization rate $\gamma(t) = \int d^3p\Gamma_{\mathbf{p}}(t)$, as defined in Lewenstein's work [46]. Note that in numerical calculations involving Eqs. (29) and (30) we use a filter to suppress electron returns longer than a half-cycle following ionization as the shorter trajectories are dominant in HHG in atomic gases (see Appendix C of Supplemental Material [55]).

The first mechanism, Eq. (29), resembles the Fourier transform of $\mathbf{x}(t)$ of Eq. (55) from Lewenstein's work corresponding to polarization generated by the quantum interference between the laser-accelerated continuum electron and the atomic ground state. Equation (29) differs from Lewenstein's model through the harmonic frequency factor $E_v \propto \omega_k^{1/2}$ due to vacuum fluctuations, affecting polarization buildup and HHG.

The second mechanism, Eq. (30), resembles the Fourier transform of the complex ionization rate $\gamma(t) = \int d^3p\Gamma_{\mathbf{p}}(t)$ of Eq. (52) of Lewenstein's work [46]. Unlike the time-dependent dipole $\mathbf{x}(t)$ found in the first channel, Eq. (29), this source was not studied there as a source of HHG. Equation (30) allows HH emission through (1) ionization nonlinearities from $\Gamma_{\mathbf{p}}(t)$ and (2) from dressing of the continuum electron as a coherent state, quantified by the parameter $\bar{\sigma}_\kappa(t)$ [44]. The formalism and the equations introduced up to now have been derived in Ref. [43]. There, the focus was on HH emission resulting from Eq. (29). Below, we analyze HH emission from Eq. (30), and we formally show the correspondence with intraband and interband currents.

B. Connection to interband and intraband HHG in solids

Although links between the quantum optical channels in Eqs. (29) and (30) and Lewenstein's work are established, there is a broader connection between quantum optical and semiclassical models. By using properties of Fourier transforms and integration by parts (see Sec. III of the Supplemental Material [55]), Eqs. (29) and (30) can be rewritten as

$$h'_\kappa = \frac{i\eta_k \mathbf{e}_\kappa}{\hbar} e^{-i\mathbf{kx}} \int_{-\infty}^{\infty} dt\, e^{i\omega_k t} \mathbf{j}_{er}(t), \tag{33}$$

$$h''_\kappa \approx \frac{i\eta_k \mathbf{e}_\kappa}{\hbar} e^{-i\mathbf{kx}} \int_{-\infty}^{\infty} dt\, e^{i\omega_k t} \mathbf{j}_{ra}(t), \tag{34}$$

where

$$\mathbf{j}_{er}(t) = |e|\dot{\mathbf{x}}(t), \tag{35}$$

$$\mathbf{j}_{ra}(t) = \int d^3p\,\mathbf{v}(\mathbf{p}_t)|b_{\mathbf{p}}(t)|^2 \tag{36}$$

represent the time-dependent interband and intraband currents, respectively. Such currents were previously studied semiclassically as mechanisms of HHG in solids [12,49,50]. Here, we define $\dot{\mathbf{x}}(t) = \partial_t \mathbf{x}(t)$, as the time-dependent dipole velocity, $\mathbf{v}(\mathbf{p}_t) = \nabla_{\mathbf{p}}(\mathbf{p}^2/2m)|_{\mathbf{p}=\mathbf{p}_t} = \mathbf{p}_t/m$ as the continuum velocity, and $|b_{\mathbf{p}}(t)|^2$ as the electronic continuum population with continuum amplitude $b_{\mathbf{p}}(t) = ie^{-iS(t)}\int_{-\infty}^{t} dt'\Omega(t')e^{iS(t')}$, of the ground-continuum wavefunction as in Ref. [46].

We observe that the quantum optical results of Eqs. (33) and (34) consist of semiclassical currents times a factor with $\eta_\kappa \propto \omega_k^{-1/2}$ resulting from vacuum fluctuations. So far, no studies have examined the relation between these two mechanisms in atoms, which is analogous to interband and intraband HHG in solids.

To clarify how the interband current [Eq. (35)] and intraband current [Eq. (36)] defined for gases relate to the theory of solids, we assume a simple two-band, single-active electron bulk solid model [12,58]. Such a model provides a simple template to qualitatively examine the physics in comparison with atomic gases. We note, however, that such a model is limited quantitatively due to its neglect of additional physics such as many-body effects. These effects include noise that can modify ionization [59] and, further, HHG [60]. Furthermore, excitonic effects, such as those analyzed using *ab initio* methods in Ref. [61], are ignored here. Finally, for a survey of effects in more complex systems and quantum materials, we refer the reader to the review article Ref. [14].

In order to facilitate the demonstration of these connections, let us write here some correspondences between atomic gas systems and two-band solid systems:

$$\mathbf{p} \to \mathbf{k} \in \mathrm{BZ}, \tag{37a}$$

$$E_0 + \frac{\mathbf{p}^2}{2m} \to \varepsilon(\mathbf{k}) = E_c(\mathbf{k}) - E_v(\mathbf{k}), \tag{37b}$$

$$\mathbf{v}(\mathbf{p}) \to \mathbf{v}(\mathbf{k}) = \hbar^{-1}\nabla_{\mathbf{k}}\varepsilon(\mathbf{k}), \tag{37c}$$

$$\mathbf{d}(\mathbf{p}) \to \mathbf{d}(\mathbf{k}) = i\int d^3\mathbf{x}\, u^*_{c,\mathbf{k}}(\mathbf{x})\nabla_{\mathbf{k}} u_{v,\mathbf{k}}(\mathbf{x}). \tag{37d}$$

That is, ionized electronic momentum $\mathbf{p}$ is replaced with the crystal wavevector $\mathbf{k}$ (or crystal momentum $\hbar\mathbf{k}$) within the Brillouin zone (BZ), where all physics for $\mathbf{k} \notin \mathrm{BZ}$ can be remapped to. Further, the atomic ground state and electronic continuum energies are replaced with the valence band $E_v(\mathbf{k})$ and the conduction band $E_c(\mathbf{k})$, respectively. $\varepsilon(\mathbf{k})$ describes the energy difference between these two bands. The continuum electronic velocity $\mathbf{v}(\mathbf{p}) = \mathbf{p}/m$ is analogous to the band difference velocity, or more simply, the band velocity $\mathbf{v}(\mathbf{k})$. Note that both the valence and conduction bands have velocities associated with them due to their curvatures in $\mathbf{k}$ space. This is not the case with an atomic system where only the ionized electron motion contributes to the system's velocity. Finally, the ground-continuum transition dipole $\mathbf{d}(\mathbf{p})$ in a gas is replaced with the valence-conduction transition dipole $\mathbf{d}(\mathbf{k})$, as in Eq. (37d), where $u_{m,\mathbf{k}}(\mathbf{x})$, $m = v, c$ are Bloch functions that correspond to periodic parts of crystal wavefunctions.

Next, with the connections established of Eq. (37), the interband current is generated by polarization accumulation due to dipole coupling of valence and conduction bands $\mathbf{d}(\mathbf{k})$. In gases, the intraband is term related to the Brunel mechanism [52]. In a solid, as the band velocity $\mathbf{v}(\mathbf{k})$ is in general a nonlinear function of $\mathbf{k}$, intraband HHG is driven by ionization and band velocity nonlinearities [12,58].

V. HIGH-HARMONIC PHOTON NUMBER EXPECTATION VALUE

We explore the two HHG mechanisms in the quantum optical context, as indicated in Eqs. (29) and (30), by examining their influence on harmonic photon yield across varying wavelengths. The total photon yield is given by

$$\langle\hat{n}\rangle = \sum_{s=1,2} \frac{V}{(2\pi)^3}\int d^3k|h_\kappa|^2. \tag{38}$$

By assuming the quantization volume $V \to \infty$, that $\mathbf{p}_t \parallel k_z$ and that one of the polarization basis vectors is contained in the plane of $\mathbf{k}$ and $\mathbf{p}_t$, we find that the photon expectation value variation with harmonic frequency, and the total yield about a given harmonic N are given by

$$\frac{d\langle\hat{n}\rangle}{d\omega_k} = \frac{V\omega_k^2}{3\pi^2c^3}|\bar{h}_\kappa|^2, \tag{39}$$

$$\langle\hat{n}\rangle_N = \frac{V}{3\pi^2c^3}\int_{(N-1/2)\omega_0}^{(N+1/2)\omega_0} d\omega_k\omega_k^2|\bar{h}_\kappa|^2, \tag{40}$$

respectively (see Sec. IVA of the Supplemental Material [55]). Here, $\bar{h}_\kappa = h_\kappa \csc\theta$ is independent of the polar angle θ with wavevector $\mathbf{k}$. In addition, note that the factor V cancels out with a factor of $1/V$ from η_κ^2 contained in $|\bar{h}_\kappa|^2$.

A. High harmonic spectra

We now investigate HHG in argon gas driven by a strong linearly polarized laser field with a Gaussian temporal envelope (full width at half maximum of 5 cycles) and a peak intensity of 3.5×10^{14} W/cm^2. The total photon yield is calculated as a function of harmonic order [Eq. (40)] for the two mechanisms described in Eqs. (33) and (34), using driving wavelengths of 1.05, 2.1, 3.05, and 4.2 μm, and a simple Coulomb correction factor for ionization (see Appendix E of the Supplemental Material [55] and Refs. [62,63]).

Figures 1(a) and 1(b) show the full harmonic spectra up to the harmonic cutoffs (black dashed lines), determined by the cutoff energy, $E_{\max} = E_0 + 3.17U_p$, where $U_p \approx |e|^2\mathcal{F}_0^2/4m\omega_0^2$ is the ponderomotive energy given a driving frequency ω_0 and maximum amplitude $\mathcal{F}_0$ [46,47]. Panels (c) through (f) focus on the low-order harmonics with dashed lines indicating the harmonic orders corresponding to the ionization energy for each wavelength.

Observing these spectra, the interband quantum optical channel, Eq. (29), is dominant throughout most of the spectra, especially in the HH plateaux, with cutoffs consistent with semiclassical atomic gas results [46–48,64–67].

In our argon model gas, the lowest order harmonics are driven by the intraband mechanism of Eq. (30), with intraband dominance increasing with wavelength. The intraband dominance noticeably occurs for more harmonics as wavelength is increased.

Finally, we note that experiments tend to measure HHG qualitatively, in terms of arbitrary units. Our theory is relevant for experiments that provide quantitative measurements of the signal such as using HH photon counts. According to the theory, we have outlined, the vacuum field HH frequency scale factor is a necessary component of the quantitative spectrum. Future experiments that utilize quantitative measurements could potentially detect the effect of the vacuum scale factor.

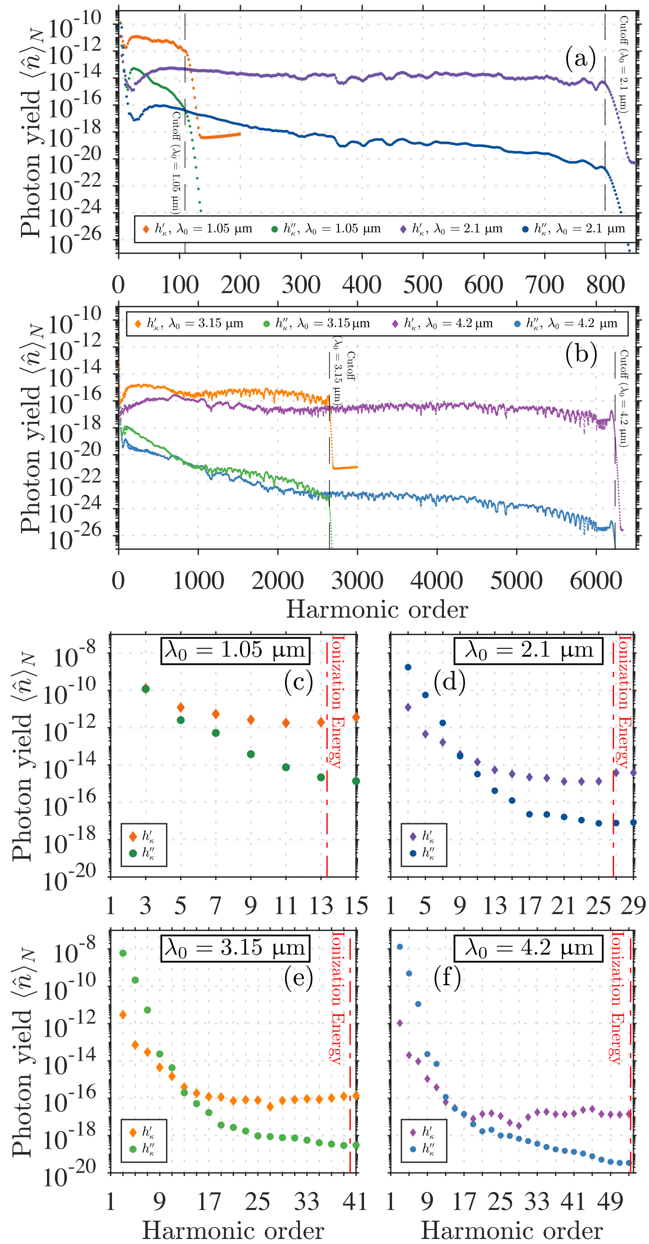

FIG. 1. Harmonic spectra, calculated via Eq. (40), for wavelengths 1.05 μm (a), (c), 2.1 μm (a), (d), 3.15 μm (b), (e), and 4.2 μm (b), (f), using a Gaussian temporal pulse (5-cycle temporal FWHM) with intensity 3.5×10^{14}W/cm^2 in argon gas. Panels (a), (b) show full spectra up to the harmonic cutoffs (black dashed lines), while panels (c)–(f) focus on spectra below the ionization energy (vertical red lines). h'_κ (interband) mechanism: orange (1.05, 3.15 μm) and purple (2.1, 4.2 μm) diamonds. h''_κ (intraband) mechanism: green (1.05, 3.15 μm) and blue (2.1, 4.2 μm) circles.

B. Harmonic of crossover of dominant HHG source

To compare the quantum optical intraband and interband analogous mechanisms as a function of the driving laser's wavelength, we plot the "crossover harmonic" (the highest harmonic where the h''_κ spectrum is greater than or equal to the h'_κ spectrum) in Fig. 2 based on Fig. 1. A linear trend of one plus the crossover harmonic with laser wavelength is observed, amounting to a constant photon energy of 5.195 eV. This allows for predicting where the intraband mechanism will dominate, enabling experiments in gas to explore and tune the dominant mechanism.

C. Crossover harmonic and the Keldysh parameter

We now explore how the crossover harmonic might depend on the ionization regime. The Keldysh parameter, $\gamma = \omega_0\sqrt{2mE_0}/|e|\mathcal{F}_0$, defines the ionization regime for a gas

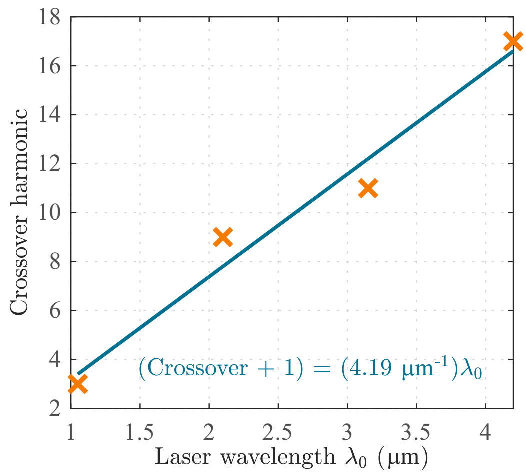

FIG. 2. Comparison of the crossover harmonic (orange crosses), defined as the highest odd harmonic for which the h''_κ (intraband) mechanism [Eq. (34)] is greater or near to equal to the h'_κ (interband) mechanism [Eq. (33)] for wavelengths as in Fig. 1. A teal linear trendline and its corresponding equation are also plotted.

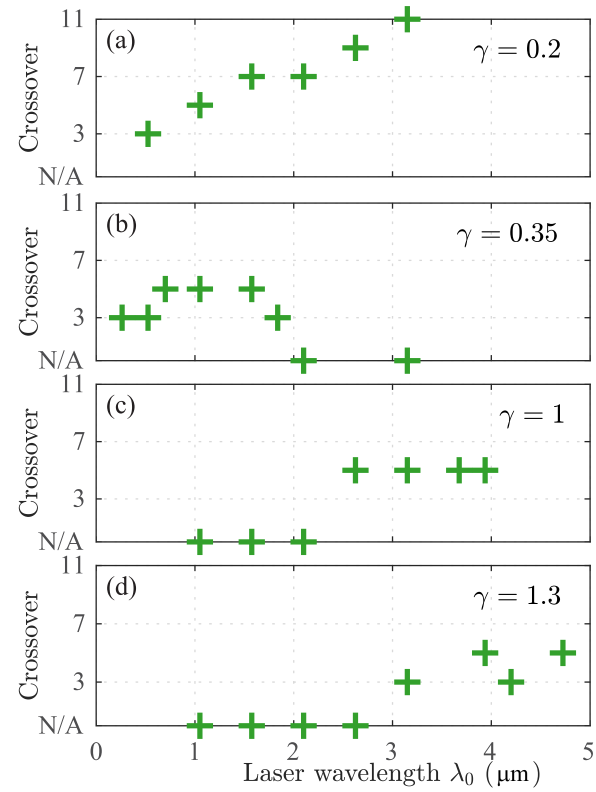

FIG. 3. Crossover harmonic variation for a sample of wavelengths for fixed Keldysh parameters, $\gamma = \omega_0\sqrt{2mE_0}/|e|\mathcal{F}_0$ as displayed in the panels. The Keldysh parameter is fixed by varying the laser field amplitude as wavelength varies. We use a 5-cycle pulse for all panels except for panel (d), where we use a 7-cycle pulse. “N/A” indicates that no crossover was seen in the range considered.

in the presence of a strong laser field [1,54]. The three regimes that are often utilized are $\gamma < 1$, $\gamma \approx 1$, and $\gamma > 1$ representing the tunneling, intermediate, and multiphoton regimes, respectively.

In Fig. 3, we analyze how the the crossover harmonic as defined in the previous subsection varies for selections of driving field wavelengths less than 5 μm for fixed Keldysh parameters within different ionization regimes. The Keldysh parameter is held constant by adjusting the laser field amplitude to account for the wavelength change. In panels (a) through (c), we use 5-cycle pulses, while in panel (d), we use a 7-cycle pulse to account for a low amplitude field at longer wavelengths.

By examining Fig. 3(a), we see that relatively deep in the tunneling regime ($\gamma = 0.2$) the crossover harmonic seems to be proportional to wavelength. As for the other three panels, demonstrating a milder tunneling regime ($\gamma = 0.35$), an intermediary regime ($\gamma = 1$) and a mild multiphoton regime ($\gamma = 1.3$), and the nature of the dependences is less clear.

Now, let us compare Fig. 3(a) with Fig. 2. We notice that both cases display apparent linear trends with wavelength. Figure 2 differs in that the laser field is fixed rather than the Keldysh parameter. There, the Keldysh parameter ranges from approximately 0.46 to approximately 0.11, with second-highest Keldysh parameter being approximately 0.23. Therefore, of the regimes shown in Fig. 3, the regimes in this figure are most like that of Fig. 3(a). Further, based on the similarity between the two trends, our results suggest that deep enough into the tunelling regime, for the wavelength range we considered, wavelength is the dominant modifier of the crossover harmonic. Due to the linear trend of crossover with wavelength, it is also related to a constant energy.

VI. CONCLUSION

In conclusion, we demonstrated that, in gases, quantizing the electromagnetic field naturally produces mechanisms analogous to semiclassical interband and intraband HHG in gases and solids. The intraband HHG term in gases is driven by the ionization nonlinearity, as the continuum does not have any nonlinear properties, unlike the valence and conduction bands in solids. The quantum optical model accounts for vacuum fluctuations, which result in an additional factor, the vacuum electric field, modifying magnitude and wavelength scaling of previous classical-light, quantum-matter theories. We found that interband analogous mechanisms dominate the HH plateau in atoms, while intraband analogous mechanisms dominate low-order harmonics. Provided the process is well into the tunneling regime, the crossover between the two channels relates to a constant photon energy independent of the wavelength of the driving laser.

DATA AVAILABILITY

The data that support the findings of this article are openly available [68].

[1] L. V. Keldysh, *Ionization in the Field of a Strong Electromagnetic Wave*, Selected Papers of Leonid V. Keldysh (World Scientific Publishing Co. Pte. Ltd., Singapore, 2023), pp. 56–63.

[2] F. H. M. Faisal, Multiple absorption of laser photons by atoms, J. Phys. B: At. Mol. Phys. **6**, L89 (1973).

[3] H. R. Reiss, Effect of an intense electromagnetic field on a weakly bound system, Phys. Rev. A **22**, 1786 (1980).

[4] A. McPherson, G. Gibson, H. Jara, U. Johann, T. S. Luk, I. A. McIntyre, K. Boyer, and C. K. Rhodes, Studies of multiphoton production of vacuum-ultraviolet radiation in the rare gases, J. Opt. Soc. Am. B **4**, 595 (1987).

[5] M. Ferray, A. L' Huillier, X. F. Li, L. A. Lompre, G. Mainfray, and C. Manus, Multiple-harmonic conversion of 1064 nm radiation in rare gases, J. Phys. B: At. Mol. Opt. Phys. **21**, L31 (1988).

[6] A. L' Huillier and Ph Balcou, High-order harmonic generation in rare gases with a 1-ps 1053-nm laser, Phys. Rev. Lett. **70**, 774 (1993).

[7] A. Scrinzi, M. Yu. Ivanov, R. Kienberger, and D. M. Villeneuve, Attosecond physics, J. Phys. B: At. Mol. Opt. Phys. **39**, R1 (2006).

[8] F. Krausz and M. Ivanov, Attosecond physics, Rev. Mod. Phys. **81**, 163 (2009).

[9] P. B. Corkum and F. Krausz, Attosecond science, Nat. Phys. **3**, 381 (2007).

[10] K. Amini *et al.*, Symphony on strong field approximation, Rep. Prog. Phys. **82**, 116001 (2019).

[11] S. Ghimire, A. D. DiChiara, E. Sistrunk, P. Agostini, L. F. DiMauro, and D. A. Reis, Observation of high-order harmonic generation in a bulk crystal, Nat. Phys. **7**, 138 (2011).

[12] G. Vampa, C. R. McDonald, G. Orlando, D. D. Klug, P. B. Corkum, and T. Brabec, Theoretical analysis of high-harmonic generation in solids, Phys. Rev. Lett. **113**, 073901 (2014).

[13] S. Ghimire and D. A. Reis, High-harmonic generation from solids, Nat. Phys. **15**, 10 (2019).

[14] E. Goulielmakis and T. Brabec, High harmonic generation in condensed matter, Nat. Photon. **16**, 411 (2022).

[15] J. Park, A. Subramani, S. Kim, and M. F. Ciappina, Recent trends in high-order harmonic generation in solids, Adv. Phys. X **7**, 2003244 (2022).

[16] L. Yue and M. B. Gaarde, Introduction to theory of high-harmonic generation in solids: Tutorial, J. Opt. Soc. Am. B **39**, 535 (2022).

[17] G. Vampa, T. J. Hammond, N. Thiré, B. E. Schmidt, F. Légaré, C. R. McDonald, T. Brabec, D. D. Klug, and P. B. Corkum, All-Optical reconstruction of crystal band structure, Phys. Rev. Lett. **115**, 193603 (2015).

[18] T. T. Luu, M. Garg, S. Yu Kruchinin, A. Moulet, M. Th. Hassan, and E. Goulielmakis, Extreme ultraviolet high-harmonic spectroscopy of solids, Nature (London) **521**, 498 (2015).

[19] S. Almalki, A. M. Parks, G. Bart, P. B. Corkum, T. Brabec, and C. R. McDonald, High harmonic generation tomography of impurities in solids: Conceptual analysis, Phys. Rev. B **98**, 144307 (2018).

[20] A. A. Lanin, E. A. Stepanov, A. B. Fedotov, and A. M. Zheltikov, Mapping the electron band structure by intraband high-harmonic generation in solids, Optica **4**, 516 (2017).

[21] D. Wu, L. Li, Y. Zhan, T. Huang, H. Cui, J. Li, P. Lan, and P. Lu, Determination of transition dipole moments of solids with high-order harmonics driven by multicycle ultrashort pulses, Phys. Rev. A **105**, 063101 (2022).

[22] H. B. Banks, Q. Wu, D. C. Valovcin, S. Mack, A. C. Gossard, L. Pfeiffer, R.-B. Liu, and M. S. Sherwin, Dynamical birefringence: Electron-Hole recollisions as probes of Berry curvature, Phys. Rev. X **7**, 041042 (2017).

[23] T. T. Luu and H. J. Wörner, Measurement of the berry curvature of solids using high-harmonic spectroscopy, Nat. Commun. **9**, 916 (2018).

[24] Y.-Y. Lv *et al.*, High-harmonic generation in Weyl semimetal β-WP_2 crystals, Nat. Commun. **12**, 6437 (2021).

[25] A. M. Parks, J. V. Moloney, and T. Brabec, Gauge invariant formulation of the semiconductor Bloch equations, Phys. Rev. Lett. **131**, 236902 (2023).

[26] M. L. Bera, J. O. De Almeida, M. Dziurawiec, M. Płodzień, M. M. Maśka, M. Lewenstein, T. Grass, and U. Bhattacharya, Topological phase detection through high-harmonic spectroscopy in extended Su-Schrieffer-Heeger chains, Phys. Rev. B **108**, 214104 (2023).

[27] C. Heide *et al.*, Probing topological phase transitions using high-harmonic generation, Nat. Photon. **16**, 620 (2022).

[28] N. Tsatrafyllis, I. K. Kominis, I. A. Gonoskov, and P. Tzallas, High-order harmonics measured by the photon statistics of the infrared driving-field exiting the atomic medium, Nat. Commun. **8**, 15170 (2017).

[29] M. Lewenstein, M. F. Ciappina, E. Pisanty, J. Rivera-Dean, P. Stammer, Th. Lamprou, and P. Tzallas, Generation of optical Schrödinger cat states in intense laser–matter interactions, Nat. Phys. **17**, 1104 (2021).

[30] J. Rivera-Dean, P. Stammer, E. Pisanty, Th. Lamprou, P. Tzallas, M. Lewenstein, and M. F. Ciappina, New schemes for creating large optical Schrödinger cat states using strong laser fields, J. Comput. Electron. **20**, 2111 (2021).

[31] S. Lemieux, S. A. Jalil, D. N. Purschke, N. Boroumand, T. J. Hammond, D. Villeneuve, A. Naumov, T. Brabec, and G. Vampa, Photon bunching in high-harmonic emission controlled by quantum light, Nat. Photon. **19**, 767 (2025).

[32] Á. Gombköto, P. Földi, and S. Varró, Quantum-optical description of photon statistics and cross correlations in high-order harmonic generation, Phys. Rev. A **104**, 033703 (2021).

[33] J. Rivera-Dean, P. Stammer, A. S. Maxwell, Th. Lamprou, P. Tzallas, M. Lewenstein, and M. F. Ciappina, Light-matter entanglement after above-threshold ionization processes in atoms, Phys. Rev. A **106**, 063705 (2022).

[34] J. Sloan, A. Gorlach, M. E. Tzur, N. Rivera, O. Cohen, I. Kaminer, and M. Soljačić, Entangling extreme ultraviolet photons through strong field pair generation, arXiv:2309.16466.

[35] D. Theidel *et al.*, Evidence of the quantum optical nature of high-harmonic generation, PRX Quantum **5**, 040319 (2024).

[36] S. Yi, N. D. Klimkin, G. G. Brown, O. Smirnova, S. Patchkovskii, I. Babushkin, and M. Ivanov, Generation of massively entangled bright states of light during harmonic generation in resonant media, Phys. Rev. X **15**, 011023 (2025).

[37] P. Stammer, J. Rivera-Dean, A. S. Maxwell, T. Lamprou, J. Argüello-Luengo, P. Tzallas, M. F. Ciappina, and M. Lewenstein, Entanglement and squeezing of the optical field modes in high harmonic generation, Phys. Rev. Lett. **132**, 143603 (2024).

[38] M. Even Tzur, M. Birk, A. Gorlach, M. Krüger, I. Kaminer, and O. Cohen, Photon-statistics force in ultrafast electron dynamics, Nat. Photon. **17**, 501 (2023).
[39] A. Rasputnyi, Z. Chen, M. Birk, O. Cohen, I. Kaminer, M. Krüger, D. Seletskiy, M. Chekhova, and F. Tani, High-harmonic generation by a bright squeezed vacuum, Nat. Phys. **20**, 1960 (2024).
[40] J. Heimerl, A. Mikhaylov, S. Meier, H. Höllerer, I. Kaminer, M. Chekhova, and P. Hommelhoff, Multiphoton electron emission with non-classical light, Nat. Phys. **20**, 945 (2024).
[41] M. Even Tzur and O. Cohen, Motion of charged particles in bright squeezed vacuum, Light Sci. Appl. **13**, 41 (2024).
[42] A. Gorlach, M. E. Tzur, M. Birk, M. Krüger, N. Rivera, O. Cohen, and I. Kaminer, High-harmonic generation driven by quantum light, Nat. Phys. **19**, 1689 (2023).
[43] N. Boroumand, A. Thorpe, G. Bart, L. Wang, D. N. Purschke, G. Vampa, and T. Brabec, Quantum engineering of high harmonic generation, arXiv:2505.22536.
[44] S. Varró, Quantum optical aspects of high-harmonic generation, Photonics **8**, 269 (2021).
[45] A. Gorlach, O. Neufeld, N. Rivera, O. Cohen, and I. Kaminer, The quantum-optical nature of high harmonic generation, Nat. Commun. **11**, 4598 (2020).
[46] M. Lewenstein, Ph Balcou, M. Yu Ivanov, A. L' Huillier, and P. B. Corkum, Theory of high-harmonic generation by low-frequency laser fields, Phys. Rev. A **49**, 2117 (1994).
[47] P. B. Corkum, Plasma perspective on strong field multiphoton ionization, Phys. Rev. Lett. **71**, 1994 (1993).
[48] K. J. Schafer, B. Yang, L. F. DiMauro, and K. C. Kulander, Above threshold ionization beyond the high harmonic cutoff, Phys. Rev. Lett. **70**, 1599 (1993).
[49] G. Vampa and T. Brabec, Merge of high harmonic generation from gases and solids and its implications for attosecond science, J. Phys. B: At. Mol. Opt. Phys. **50**, 083001 (2017).
[50] A. Thorpe, N. Boroumand, A. M. Parks, E. Goulielmakis, and T. Brabec, High harmonic generation in solids: Real versus virtual transition channels, Phys. Rev. B **107**, 075135 (2023).
[51] A. M. Parks, G. Ernotte, A. Thorpe, C. R. McDonald, P. B. Corkum, M. Taucer, and T. Brabec, Wannier quasi-classical approach to high harmonic generation in semiconductors, Optica **7**, 1764 (2020).
[52] F. Brunel, Harmonic generation due to plasma effects in a gas undergoing multiphoton ionization in the high-intensity limit, J. Opt. Soc. Am. B **7**, 521 (1990).
[53] F. Krausz and T. Brabec, Intense few-cycle laser fields: Frontiers of nonlinear optics, Rev. Mod. Phys. **72**, 545 (2000).
[54] N. Boroumand, A. Thorpe, A. M. Parks, and T. Brabec, Keldysh ionization theory of atoms: Mathematical details, J. Phys. B: At. Mol. Opt. Phys. **55**, 213001 (2022).
[55] See Supplemental Material at http://link.aps.org/supplemental/10.1103/8lhh-gq58 for detailed information of the ground state photon wavefunction derivation and its connections to interband and intraband currents of solids. Methods of expectation value calculations are also given there.
[56] A.-M. Wazwaz, *Linear and Nonlinear Integral Equations: Methods and Applications* (Higher Education Press, Beijing and Springer-Verlag GmbH Berlin Heidelberg Springer e-books, Berlin, Heidelberg, 2011).
[57] R. M. Wilcox, Exponential operators and parameter differentiation in quantum physics, J. Math. Phys. **8**, 962 (1967).
[58] G. Vampa, T. J. Hammond, N. Thiré, B. E. Schmidt, F. Légaré, C. R. McDonald, T. Brabec, and P. B. Corkum, Linking high harmonics from gases and solids, Nature (London) **522**, 462 (2015).
[59] N. Boroumand, A. Thorpe, G. Bart, A. M. Parks, M. Toutounji, G. Vampa, T. Brabec, and L. Wang, Strong field physics in open quantum systems, Rep. Prog. Phys. **88**, 070501 (2025).
[60] L. Wang, A. M. Parks, A. Thorpe, G. Bart, and T. Brabec, Quantum dial for high-harmonic generation, arXiv:2509.13518.
[61] V. Chang Lee, L. Yue, M. B. Gaarde, Y. Chan, and D. Y. Qiu, Many-body enhancement of high-harmonic generation in monolayer MoS_2, Nat. Commun. **15**, 6228 (2024).
[62] N. Milosevic, V. P. Krainov, and T. Brabec, Relativistic theory of tunnel ionization, J. Phys. B: At. Mol. Opt. Phys. **35**, 3515 (2002).
[63] M. V. Ammosov, N. B. Delone, and V. P. Krainov, Tunnel ionization of complex atoms and of atomic ions in an alternating electromagnetic field, Sov. J. Exp. Theor. Phys. **64**, 1191 (1986).
[64] C.-G. Wahlström, J. Larsson, A. Persson, T. Starczewski, S. Svanberg, P. Salières, Ph Balcou, and A. L' Huillier, High-order harmonic generation in rare gases with an intense short-pulse laser, Phys. Rev. A **48**, 4709 (1993).
[65] C. Jin and C. D. Lin, Comparison of high-order harmonic generation of ar using truncated Bessel and Gaussian beams, Phys. Rev. A **85**, 033423 (2012).
[66] S. Majidi, R. Aghbolaghi, H. A. Navid, and R. Mokhlesi, Optimization of cut-off frequency in high harmonic generation in noble gas, Appl. Phys. B **130**, 11 (2024).
[67] S. Chintalwad, T. Chau, and L. V. Dao, Cascaded high harmonic generation in mixture of argon and helium: Achieving a broad photon spectrum, Phys. Plasmas **31**, 123301 (2024).
[68] A. Thorpe, N. Boroumand, G. Bart, L. Wang, G. Vampa, and T. Brabec, Dataset: A unified treatment of high-harmonic generation in gases and solids, Zenodo (2025), doi:http://doi.org/10.5281/zenodo.17528862.